Precambrian crystalline basement properties from pressure history matching and implications for induced seismicity in the US midcontinent

Authors: E. Ansari[1] and T.S. Bidgoli[2]

Affiliations:

[1]1030 Jana Dr, Lawrence, KS, 66049, USA

[2]Department of Geological Sciences, University of Missouri, Columbia, Missouri 65211, USA

Corresponding author: Tandis S. Bidgoli (bidgolit@missouri.edu)

Key Points:

- A 3D geological and history-matched numerical model for south-central Kansas constrains the hydrological properties of the basement
- Basement properties from pressure history matching account for distributed fault and fracture networks
- Basement diffusivities are substantially lower that those derived from earthquake triggering fronts across the model area

Keywords: induced seismicity, Kansas and Oklahoma earthquakes, wastewater injection, rbuckle aquifer, crystalline basement

Abstract

Injection-induced seismicity across the US midcontinent has almost exclusively occurred in the crystalline basement that underlies the Arbuckle Group aquifer and its equivalents, the primary wastewater disposal zone in this region. However, the properties of the basement are not well known. Newly compiled data, from Class I wells in Kansas, provide a unique record of pressures in the Arbuckle and an opportunity to constrain the reservoir-scale properties of the basement such as permeability, diffusivity, and specific storage. Constraints on these parameters are critical for modeling fluid flow and pressures across the entire Arbuckle-basement system, and are necessary for accurate evaluation and prediction of injection-induced earthquakes. Here, we present a detailed, three-dimensional geological and pressure history-matched numerical model for the Arbuckle and basement, based on data from >400 wells covering a large region in south-central Kansas, where injection-induced seismicity has been concentrated since 2014. Simulations of dynamic data from 319 wells indicate that Arbuckle pressures have increased by 1.1 MPa in high injection rate areas and an overpressure of <0.1 MPa may be the cause of seismicity in the basement. Pressure-history matching also yields the likely range in porosity (0.3-7%), permeability (0.1-0.7 mD), and diffusivity (0.004-0.07 m^2/s) for the basement. The resulting estimates suggest reservoir-scale properties of the basement are enhanced by faults and fractures. Importantly, the diffusivities determined in this study are lower than estimates derived from Kansas earthquake triggering fronts, and suggest that such seismicity-based techniques may have limitations, particularly where space-time patterns between injection and seismicity are complex.

1 Introduction

The revolution in unconventional oil and gas resource development, and associated injection of coproduced wastewater into deep aquifers, has increased seismicity rates across the US midcontinent over the last decade (Ellsworth, 2013; Langenbruch & Zoback, 2016; Weingarten et al., 2015). Although the target disposal zone in this region is the Cambrian-Ordovician Arbuckle Group (herein referred to as the Arbuckle) and age equivalent saline aquifers, the seismicity has almost exclusively occurred in the underlying Precambrian crystalline basement. These earthquakes have illuminated a complex network of faults below the sedimentary cover that can slip under small stress changes; however, the hydrologic characteristics of the basement are not

well known, due, in part, to a dearth of data. Kansas, for example, has more than 400,000 oil and gas wells, but less than 1% penetrate the basement and of those, only 15% percent extend more than 20 m into it. Fewer still have well log and core data, and it's not clear if the limited data that exist are representative of the average reservoir-scale hydrologic properties of the basement. The hydrogeological characteristics of the basement are essential for modeling the pressure evolution from the overlying Arbuckle aquifer and its relationship to midcontinent seismicity.

Seismicity in the Kansas and Oklahoma occurs at a median depth of 6.5 km below the surface and continues down to ~10 km depth (Schoenball & Ellsworth, 2017) (Figure S1). The ubiquity of these earthquakes across these states and their substantial depth below the Arbuckle suggest that hydraulically conductive basement faults are widespread and may be enhancing the average reservoir-scale properties of the basement such as porosity, permeability, diffusivity, and specific storage. The crystalline basement in intraplate settings is known to have an average permeability three to four orders of magnitude higher than that measured on core samples (Townend & Zoback, 2000). Although this scale dependence for permeability (and storage) has been confirmed by meta-analysis of global in situ permeability measurements from shallow (< 2 km depth) basement (Ranjram et al., 2016), relationships in the deeper basement are not well established. Lacking needed measurements, many researchers have used earthquake triggering fronts (Shapiro et al., 1997; Goebel et al., 2017; Peterie et al., 2018; Schoenball et al., 2018) to estimate the basement properties, resulting in a wide range of values (Table 1). For example, Schoenball et al. (2018) use the earthquake front concept for tracking seismicity diffusion in the vicinity of a wellbore and calculate a hydraulic diffusivity range of 0.012-0.06 m^2/s for the basement, while Peterie et al. (2018) use the same concept to calculate a hydraulic diffusivity of 7 m^2/s and conclude that seismicity diffuses far-field (> 90 km) of causal wells. The modeling efforts in Table 1 report reservoir-scale average values and reason that injection occurs over a broad spatial extent, densely covered by wells (2 to 5 km spacing), that results in pressure communication between wells and thus justifying the large-scale of analysis.

Here, we use geological modeling and pressure history matching to characterize the porosity, permeability, diffusivity, and specific storage of the crystalline basement in south-central Kansas, where injection-induced earthquakes have been concentrated since 2014 and limited data on the basement are available. We take advantage of available well log, core, and dynamic data

(injection volumes and pressures) for the Arbuckle to develop numerical models that fix the aquifer's properties with different geological realizations. The fixed models are used to optimize the basement properties by matching pressure data measured in the Arbuckle. The approach is also useful for understanding pressure transmission into the basement and its relationship with midcontinent seismicity.

Table 1. Hydrologic properties of the Precambrian basement reported for the central US

Source	Basement porosity (fraction)	Basement permeability ($\times 10^{-15}$ m^2)	Basement storage (m^{-1})	Basement diffusivity (m^2/s)
Zhai et al., 2020	-	-	-	0.0001
Dempsey & Riffault, 2019	0.01	0.32-0.47	-	0.26-0.37
Peterie et al., 2018	-	-	-	7
Langenbruch et al., 2018 [a]	0.01	2	1×10^{-7}	0.38
Goebel et al., 2017 [b]	-	-	1.18×10^{-7}	0.05-0.1
Schoenball et al., 2018 [c]	-	0.01-1	-	0.012-0.06
Zhang et al., 2013 [d]	-	0.02	10^{-7}	NA
Keranen et al., 2014 [e]	-	-	10^{-6}	0.0001-0.01
Zhang et al., 2016 [f]	-	1	10^{-6}	0.01-1

[a] Permeability obtained by matching pressure profile and seismicity rate at 6.5 km depth. They obtain basement porosity value from Freeze & Cherry, 1979. Diffusivity is derived from their reported values.
[b] These values are for basement faults and assume negligible diffusivity for the bulk. They use seismicity migration and attribute obtained diffusivity values of 0.1 to 2 m^2/s to the Arbuckle aquifer.
[c] They use seismicity migration to calculate diffusivity values for the basement fault system.
[d] They have reported a vertical permeability of 10^{-13} m^2 for the basement faults.
[e] They assume a depth-decreasing basement diffusivity of 0.01 m^2/s at the top and 0.0001 at the bottom.
[f] Assigning a diffusivity range of 0.01-01 m^2/s to the basement bulk and diffusivity of $0.1 - 1$ m^2/s to the fault zone reproduced the pressure needed to trigger seismicity at depth.

2 Background

49 Class I and 2,381 Class II wells inject wastewater into the Arbuckle aquifer across Kansas (Figure 1). Class I wells refer to UIC (Underground Injection Control) wells that inject industrial waste fluids, commonly under gravity (no pump pressure), following a strict set of EPA (Environmental Protection Agency) regulations, which include annual monitoring of injection zone formation pressure (P*, Text S1) via fall-off tests. The formation pressure data are unique and important because their changing rate contains the Arbuckle's response to fluctuations in wastewater injection and are valuable for understanding flow mechanisms in the aquifer and their relationship to observed seismicity.

3 Data and Methods

3.1 Geological-simulation models and data

A geological model of the Arbuckle and basement was constructed in Schlumberger's Petrel™ (Text S2, Figure S1). The model area, shown in Figure 1, is approximately 152 km in the X (longitude) and 118 km in the Y (latitude) directions, and consists of twelve Arbuckle and five basement layers (Figure S2; Table S1). The structure and layering of the Arbuckle were established from formation tops and log correlation for 486 wells in the area. The Arbuckle thickness ranges between 245 m to 365 m in the area, with a depth ranging from 348 m to 1330 m subsea. The porosity in the Arbuckle is inferred from core measurements in four wells and the permeability is inferred from drill-stem tests in three wells (Figure 1). A layer of low-permeability baffle, interpreted from well-logs, separates the upper and lower Arbuckle and reduces the vertical hydraulic connection in the aquifer (Hearn et al., 2018). We used sequential Gaussian simulation to create five geological realizations of the aquifer and distributed porosity and permeability in the grid blocks (Figure S2, Tables S2-S11). Arbuckle porosities and permeabilities range from $0.018 - 0.089$ and $3 - 2580$ mD, respectively. The basement consists of five layers (1.2 km thick) that follow the Arbuckle structure. The porosity and permeability of the basement are assumed to be uniform and homogeneous, and obtained by history matching the pressure for several key Class I wells (described below).

We use the geological model to simulate dynamic data from Arbuckle wells since 2000. The injection volumes come from 319 Class I and II wells in south-central Kansas. For Class I wells, we use the annual injection volumes, obtained by summing reported monthly injection volumes data. For Class II wells, we used the reported annual volumes. Pressure data used for history matching were obtained from annually performed pressure fall-off tests (Text S1) from three Class I wells in the model area, KS-01-077-002 in Harper County and KS-01-173-001 and -002 in Sedgwick County, which are adjacent to one another (<100 m apart) (Ansari et al., 2019; Ansari and Bidgoli, 2020). The Computer Modeling Group (CMG) IMEX simulator (CMG-IMEX User Manual, 2016) was used for dynamic flow modeling and CMG CMOST (CMG-CMOST User Manual, 2016) was used for matching the modeled data to the measured pressure at the Class I wells and for calculating the basement porosity and permeability. After basement properties were

obtained, the cumulative pressure change and pressure rate in the Arbuckle and at hypocentral depths in the basement were obtained.

3.2 Numerical history matching

Basement properties were calculated using two different models: (A) a finite extent basement with large thickness and no leakage at the bottom and (B) a basement connected to a leaking analytical aquifer at the bottom boundary. The difference between the two model types is that the numerically discretized finite basement with large thickness in the first model type is connected to an analytical aquifer model with the same petrophysical properties (permeability and porosity) to account for its infinite thickness.

(A) Finite aquifer with no leakage at the bottom: This approach has been used by Langenbruch et al. (2018) and assumes a numerical discretization for a large thickness basement. We use Neumann-Type (no-flow) boundary conditions for all outer boundaries including the bottom of basement and explore the pressure distribution in the reservoir and and deep basement (up to ~7.5 km depth).

(B) Basement connected to a leaking analytical aquifer at the bottom boundary: The previous model is further improved by connecting an analytical aquifer with leakage (Carter-Tracy model, Dake, 2008) to the bottom of the basement to represent the infinite capacity and extent of the basement at the bottom side (Text S3; Figures S3 and S4). The permeability and porosity of this analytical aquifer are the same as values for the numerically discretized basement and found during the history matching process. Other sides of the model are considered as Neuman-Type (no flow boundary condition), similar to the previous model. The flow leaks from the Arbuckle into the numerical (gridded) basement, and from the basement into the analytical basement aquifer, when the pressure is high in each of the formations, to assure a pressure equilibrium in the entire model.

Table S12 summarizes the Arbuckle properties used for numerical simulations of both model types (following Langenbruch et al., 2018). Injection starts in the year 2000 and the three Class I wells are history matched using CMG particle swarm optimization method (Text S5). The basement is assumed to be isotropic and the search space for its properties is summarized in Table S13.

4 Results

Figure S2 shows the 3D porosity and permeability distributions in the Arbuckle aquifer for the five geological realizations. To obtain a pressure history match for these realizations of the geocellular model, the basement porosity and permeability are adjusted and tuned using each model type (A and B) through more than 2000 iterative simulation runs. The process is illustrated in Figure 2, which shows the historical pressure data (blue points), iterative runs (light blue curves), and the best-fit model (red curve). The error term for each well is defined as the sum of squares of the difference between the blue points (observations) and the red line (prediction). The best-fit model is determined by minimizing the sum of the error terms for all three wells combined. While the optimization algorithm finds a best-fit for all of the wells, for well KS-01-077-002 (Figure 2a), the best-fit model is better aligned with the pressure measurements than in the other two wells (Figure 2b and 2c). Note that this is likely a consequence of differences in injection at each well site. Injection into well KS-01-077-002 is relatively low and the recorded pressure increase mostly reflects high regional injection in southern Kansas. In contrast, the best-fit model for wells KS-01-173-001 and KS-01-173-002, which are in close proximity to one another, has a poorer match to the measured data because these wells experience substantially higher in-well disposal. Additionally, several other high-rate Class I injection wells are in close proximity to these wells (Ansari et al. (2019). These results are aligned with Zhai et al. (2020), who also argue that local injection is the likely cause of excessive pressure increase observed in well KS-01-173-002.

Figure 3 summarizes the results obtained from history matching all realizations (types A and B). The specific storage (S_s) and diffusivity (D) were determined using the values in Table S12 and solving:

$$S_s = \rho_{fl} g \left(\phi \beta_{fl} + \beta_r \right)$$

$$D = \frac{k \, \rho_{fl} \, g}{\eta \, S_s}$$

in which, ϕ is porosity, ρ_{fl} is fluid density, β_{fl} and β_r stand for bulk compressibility of water and rock, k is permeability, η is fluid viscosity, and g is the gravitational acceleration. Overall, the pressure history match yields low porosity (0.3-7%), permeability (0.1-0.7 mD), and diffusivity ($0.004 - 0.07\ m^2/s$) values for the basement (summarized in Table S14).

Figure 4 shows an example of the numerical simulation results with our basement properties established from the history matching (see model 3, Table S14). The figure shows that pressure increase affects an extensive area in south-central Kansas, peaking at ≈1.1 MPa in 2015 and decreasing in 2016 while further diffusing into the basement. Although the pressure starts to decrease in the Arbuckle after 2015, the pressure in the basement increases because of a pressure diffusion time lag (Schoenball et al., 2018). The total pressure increase at ≈1.8 km below the top of basement (thickness of basement grid blocks are 1.2 km) remains elevated in 2015 and 2016 at <0.5 MPa. By comparison, the pressure rate in both the Arbuckle and the basement peaks in 2014 and decreases in 2015 and 2016. The pressure rate in the Arbuckle maxes at ≈0.4 MPa/year in 2014. The pressure rate maxes at ≈0.2 MPa/year at ≈0.6 km average depth below the top of the basement and <0.1 MPa/year in deeper areas in 2014, and slowly drops to <0.1 MPa/year in 2016. Similar results were obtained with all model realizations.

5. Discussion

Unlike previously published works that fine-tune the Arbuckle's properties using seismicity rates (Dempsey & Riffault, 2019; Langenbruch et al., 2018), we use available well data, including vital Class I pressure data, and modeling to characterize the Arbuckle. The resulting 3D pressure history matched models (e.g., Figure 4) yield representations of the pressure change magnitude and distribution in the Arbuckle and basement. The simulation results indicate that pressure increases peak at ≈1.1 MPa in the Arbuckle and then fall in 2016, following both state-mandated and market-driven reductions in wastewater disposal. The pressure distributions suggest a coalesced pressure plume in the Arbuckle aquifer, a consequence of pressure interference between wells due to the high permeability and diffusivity of the Arbuckle, consistent with the results of Langenbruch et al. (2018) and Dempsey & Riffault (2019).

The pressure distributions provided in Figure 4, and produced in other realizations of the model, are also in line with the seismicity trends in the state. Seismicity in southern Kansas peaked in 2015 and dropped in 2016 (Rubinstein et al., 2018), a pattern also confirmed by physics-based hydromechanical and seismicity rate models (Zhai et al., 2020). Further, the results suggest that pressure rate is the dominant control on the seismicity rate (see Figure 4c-f where pressure rate in the basement increases in 2015 relative to 2014 and then drops in 2016, despite elevated cumulative pressure). However, the cumulative pressure increase due to historical injection makes

faults susceptible to smaller pressure changes and thus, decreases the minimum pressure required to initiate seismicity. Another important insight is that cumulative pressure increases can reach farther distances than the changes in pressure rate, which appear to stay confined to areas near injection wells. This may imply that for mitigation of induced earthquakes, regulating wells proximal (<30 km distance) to an earthquake source should be prioritized over distant wells.

Our results indicate that the cumulative pressure increase at 4.5 km below the top of the basement in south-central Kansas is <0.1 MPa, which is lower than the values reported by Schoenball et al. (2018), who find that pressure at this depth in Guthrie-Langston region of Oklahoma has steadily increased since injection began in 2002, reaching ≈0.2-0.3 MPa in 2011. However, similar to their work, we also observe that the large permeability contrast between the Arbuckle and basement delays the onset of pressure decay to hypocentral depths. Nevertheless, our results are consistent with prior studies that have found that stress changes of 0.01 to 0.1 MPa in the basement are sufficient to trigger near-failure fault slip and induce seismicity (Gomberg & Johnson, 2005; Keranen et al., 2014; Rubinstein et al., 2007).

The basement properties obtained from the 3D history matching are within the range of values from the studies in Table 1 and Townend and Zoback (2000), who conclude that the permeability of the upper crust is ≈0.01-0.1 mD over 1 to 10 km scales. The obtained basement properties, however, are higher than site specific data for deep crystalline rocks (Coyle and Zoback, 1988; Huenges et al., 1997; Lockner et al., 1991; Morrow and Byerlee, 1988, 1992; Morrow et al., 1994). While core, well log, and well test data provide basement properties in the vicinity of a well, such data fail to account for secondary enhancements created by faults and fractures. Importantly, these data systematically underestimate hydrological properties needed for the large scale of analysis, necessary for developing seismic hazard maps (e.g., Langenbruch et al., 2018) and for efficiently predicting seismicity rates (Dempsey & Riffault, 2019). The exception to this is porosity; our reported range is similar to the limited laboratory- and well log-based porosity estimates for the crystalline basement in the midcontinent (Freiberg et al., 2014; Kibikas et al., 2019, 2020). The consistency of results using such different scales of analysis, in part, reflects the wide range in reported values (<1% to 15%), but it may also imply that faults and fractures that enhance the other properties of the basement are volumetrically limited as a proportion of the basement.

The basement diffusivities in Table 1 range from 0.0001 m^2/s, one order of magnitude lower than our results, to 7 m^2/s, two orders of magnitude higher than our results. One reason for the wide range in published estimates is that researchers use different earthquake triggering fronts (Shapiro et al., 1997) in their calculations. For example, Peterie et al. (2018) use earthquake fronts established by the whole of the earthquake catalog in south-central Kansas to calculate a diffusivity of 7 m^2/s across the area of our model. In contrast, Schoenball et al. (2018) apply the same seismicity migration concept to discrete clusters of earthquakes along faults in Oklahoma and find a much lower diffusivity (up to 0.06 m^2/s) for the basement. Diffusivities reported here are more in line with values reported by Schoenball et al. (2018) and may imply that caution must be taken in determining diffusivities from earthquake triggering fronts, particularly where prior injection history (cumulative injection) and pressure interference from multiple wells can complicate spatial and temporal patterns in seismicity, as is the case in south-central Kansas.

6 Limitations

Our study has several limitations. The Horner false pressure (P*) obtained from fall-off tests slightly underestimates the average formation pressure and this underestimation increases with time (Ansari et al., 2019). Thus, a perfect history match may not be possible and a tolerance of 5% for the matches may be acceptable. The Arbuckle is also known to be a highly fractured and heterogeneous aquifer (Franseen et al., 2004), and likely follows a dual porosity model; however, the Horner analysis used to derive P* assumes homogenous rock properties. These limitations, however, may have negligible or secondary effects on the results because the interpretations from transient testing techniques for homogeneous reservoirs appear to be representative, even when applied to heterogeneous reservoirs, and show average values for the properties of the system (Earlougher, 1977; Horne, 1995; Lee et al., 2013).

Other intrinsic limitations of the current work relate to the sparseness of the reservoir property and pressure data, which the models and the properties of the basement are conditioned upon. Because formation pressure data are recorded in only three wells in the study area (two of which come from the same site), and these pressure profiles are sensitive to local permeability distributions and injection (Fig. 2), the inferred basement properties should be seen as large-scale averages. Thus, the obtained estimates provide lower bounds for porosity and permeability and may be biased for small-scale models (e.g., faults or local models). Additionally, our models

ignore potential heterogeneities in the basement that could be the cause of poorer pressure matches in wells KS-01-073-002 and KS-01-073-003 in Sedgwick County. The geological model is also restricted to southern Kansas and ignores high-rate disposal in Oklahoma. Although Kansas disposal was sufficient to obtain a match for well KS-01-077-002 in Harper County, the inclusion of the Oklahoma wells could improve the pressure matches for the other Class I wells and better align our results with those of Zhai et. al. (2020).

7 Conclusion

Our 3D pressure-matched models show that the Arbuckle pressure has increased up to ≈1.1 MPa in high injection rate areas near the Kansas-Oklahoma border and a pressure rate of less than 0.1/yr MPa triggers deep (>2.4 km from the top of the basement) seismicity. The history matching also yields low porosity (0.3%-7%), permeability (0.1-0.7 mD), and diffusivity ($0.004 - 0.07\ m^2/s$) values for the basement, indicating that the Arbuckle could be effectively studied using 2D analytical models. In addition, the time lag for the Arbuckle pressure changes to penetrate deep into the basement implies that seismicity does not decrease immediately post shut-in. Our results suggest that pressure rate (pressure gradient in time) controls the seismicity rate; whereas, the total pressure increase due to historical injection decreases the minimum pressure required to initiate seismicity.

Acknowledgements: We thank J. Victorine for his assistance in compiling data from Class I well reports, and C. Jackson and A. Hollenbach for assistance with Class II injection volumes data. We also thank A. Hollenbach for his geologic modeling efforts, part of his M.S. thesis research under Bidgoli. We acknowledge IHS Markit for donating licenses of Petra™, Schlumberger for donating licenses of Petrel™, and Computer Modeling Group for donating licenses of IMEX and CMOST. Funding: This material is based upon work supported by the Department of Energy under Award Number DEFE0029474 to Bidgoli.

endorsement, recommendation, or favoring by the United States Government or any agency thereof. The views and opinions of authors expressed herein do not necessarily state or reflect those of the United States Government or any agency thereof. Competing interests: Authors declare no competing interests. Data and materials availability: Class I and II well data from Kansas were provided by the Kansas Department of Health and Environment and Kansas Corporation Commission, respectively. The data are available as supplementary files in Ansari et al. (2019).

References

Ansari, A. E., Bidgoli, T. S., & Hollenbach, A. (2019). Accelerated fill-up of the Arbuckle Group aquifer and links to U.S. midcontinent seismicity. *Journal of Geophysical Research: Solid Earth*, 25. https://doi.org/10.1029/2018JB016926

Ansari, E., & Bidgoli, T. S. (2020). Reply to Comment by Peterie et al. on "Accelerated Fill- up of the Arbuckle Group Aquifer and Links to U.S. Midcontinent Seismicity." *Journal of Geophysical Research: Solid Earth*, 1–7. https://doi.org/10.1029/2019jb019275

CMG-CMOST User Manual. (2016). Computer Modeling Group Ltd. *Calgary, AB, Canada*.

CMG-IMEX User Manual. (2016). Computer Modeling Group Ltd. *Calgary, AB, Canada*.

Coyle, B. J., & Zoback, M. D. (1988). In situ permeability and fluid pressure measurements at∼ 2 km depth in the Cajon Pass research well. Geophysical Research Letters, 15(9), 1029-1032.

Dake, L. P. (1983). Fundamentals of reservoir engineering. In *Elsevier*.

Dempsey, D., & Riffault, J. (2019). Response of Induced Seismicity to Injection Rate Reduction: Models of Delay, Decay, Quiescence, Recovery, and Oklahoma. *Water Resources Research*. https://doi.org/10.1029/2018WR023587

Earlougher, R. C. (1977). Advances in Well Test Analysis. *Monograph Volume 5 - Henry L. Doherty Series*.

Ellsworth, W. L. (2013). Injection-induced earthquakes. *Science*, *341*(6142), 1225942–1225942. https://doi.org/10.1126/science.1225942

Franseen, E. K., Byrnes, A. P., Cansler, J. R., & Carr, T. (2004). *The geology of Kansas: Arbuckle*

Group. Kansas Geological Survey.

Freiburg, J. T., Morse, D. G., Leetaru, H. E., Hoss, R. P., & Yan, Q. (2014). *A depositional and diagenetic characterization of the Mt. Simon Sandstone at the Illinois Basin-Decatur Project carbon capture and storage site, Decatur, Illinois, USA.*

Gomberg, J., & Johnson, P. A. (2005). Dynamic triggering of earthquakes. *Nature*, *437*(October), 2005. https://doi.org/10.1038/nature04167

Hearn, E. H., Koltermann, C., & Rubinstein, J. L. (2018). Numerical models of pore pressure and stress changes along basement faults due to wastewater injection: Applications to the 2014 Milan, Kansas earthquake. *Geochemistry, Geophysics, Geosystems*. https://doi.org/10.1002/2017GC007194.

Horne, R. N. (1995). Modern well test analysis. Petroway Inc.

Huenges, E., Erzinger, J., Kück, J., Engeser, B., & Kessels, W. (1997). The permeable crust: Geohydraulic properties down to 9101 m depth. *Journal of Geophysical Research: Solid Earth*, 102(B8), 18255-18265.

Keranen, K. M., Weingarten, M., Abers, G. A., Bekins, B. A., & Ge, S. (2014). Sharp increase in central Oklahoma seismicity since 2008 induced by massive wastewater injection. *Science, 345*(6195), 448–451. https://doi.org/10.1126/science.1255802

Kibikas, W. M., Carpenter, B. M., & Ghassemi, A. (2019, August). The petrophysical and mechanical properties of Oklahoma's crystalline basement. In *53rd US Rock Mechanics/Geomechanics Symposium*. American Rock Mechanics Association.

Kibikas, W. M., Carpenter, B. M., & Ghassemi, A. (2020). Mechanical strength and physical properties of Oklahoma's igneous basement. *Tectonophysics*, 777, 228336.

Langenbruch, C., & Zoback, M. D. (2016). How will induced seismicity in Oklahoma respond to decreased saltwater injection rates? *Science Advances*, *2*(e1601542), 1–9. https://doi.org/10.1126/sciadv.1601542

Langenbruch, C., Weingarten, M., & Zoback, M. D. (2018). Physics-based forecasting of man-made earthquake hazards in Oklahoma and Kansas. *Nature Communications*, *9*(1), 1–10.

https://doi.org/10.1038/s41467-018-06167-4.

Lee, J., Rollins, J. B., Spivey, J. P., & Lee, W. J. (2013). Applied well test interpretation. Richardson, TX: Society of Petroleum Engineers.

Lockner, D., S. Hickman, V. Kuksenko, A. Ponomarev, A. Sidorin, J. Byerlee, and B. Khakaev (1991). Laboratory- determined permeability of cores from the Kola Superdeep Well, USSR. *Geophysical Research Letters* 18(5), 881-884.

Morrow, C., & Byerlee, J. (1988). Permeability of rock samples from Cajon Pass, California. *Geophysical Research Letters*, 15(9), 1033-1036.

Morrow, C.A., & Byerlee, J.D. (1992). Permeability of core samples from Cajon Pass scientific drill hole: Results from 2100 to 3500 m depth. *Journal of Geophysical Research* 97, 5145–5151.

Morrow, C.A., Lockner, D., Hickman, S., Rusanov, M., and Röckel, T. (1994). Effects of lithology and depth on the permeability of core samples from the Kola and KTB drill holes. *Journal of Geophysical Research*. 99, 7263–7274.

Peterie, S. L., Miller, R. D., Intfen, J. W., & Gonzales, J. B. (2018). Earthquakes in Kansas induced by extremely far-field pressure diffusion. *Geophysical Research Letters*, 1–7. https://doi.org/10.1002/2017GL076334

Peterie, S. L., Newell, K. D., Bohling, G. C., & Mandel, R. D. (2020). Comment on "Accelerated Fill- Up of the Arbuckle Group Aquifer and Links to U.S. Midcontinent Seismicity" by Ansari et al. (2019). *Journal of Geophysical Research: Solid Earth*. https://doi.org/10.1029/2019jb018348

Ranjram, M., Gleeson, T., & Luijendijk, E. (2016). Is the permeability of crystalline rock in the shallow crust related to depth, lithology, or tectonic setting? *Crustal Permeability*, 123–136. https://doi.org/10.1002/9781119166573.ch12

Rubinstein, J. L., Vidale, J. E., Gomberg, J., Bodin, P., Creager, K. C., & Malone, S. D. (2007). Non-volcanic tremor driven by large transient shear stresses. *Nature*, *448*(7153), 579–582. https://doi.org/10.1038/nature06017

Rubinstein, J. L., Ellsworth, W. L., & Dougherty, S. L. (2018). The 2013–2016 induced earthquakes in Harper and Sumner counties, Southern Kansas. *Bulletin of the Seismological Society of America, 2017*. https://doi.org/10.1785/0120170209

Schoenball, M., & Ellsworth, W. L. (2017). Waveform- relocated earthquake catalog for Oklahoma and southern Kansas illuminates the regional fault network. *Seismological Research Letters*, *88*(5), 1252–1258. https://doi.org/10.1785/0220170083

Schoenball, M., Walsh, F. R., Weingarten, M., & Ellsworth, W. L. (2018). How faults wake up: The Guthrie-Langston, Oklahoma earthquakes. *The Leading Edge*, *37*(2), 100–106. https://doi.org/10.1190/tle37020100.1

Segall, P., & Lu, S. (2015). Injection-induced seismicity: Poroelastic and earthquake nucleation effects. *Journal of Geophysical Research: Solid Earth*, *120*(7), 5082–5103. https://doi.org/10.1002/2015JB012060

Shapiro, S. A., Huenges, E., & Borm, G. (1997). Estimating the crust permeability from fluid-injection-induced seismic emission at the KTB site. *Geophysical Journal International*, *131*(2). https://doi.org/10.1111/j.1365-246X.1997.tb01215.x

Shapiro, Serge A. (2015). *Fluid-induced seismicity*. *Fluid-Induced Seismicity*. https://doi.org/10.1017/CBO9781139051132

Townend, J., & Zoback, M. D. (2000). How faulting keeps the crust strong. *Geology*, *28*(5), 399–402. https://doi.org/10.1130/0091-7613(2000)28<399:HFKTCS>2.0.CO

Weingarten, M., Ge, S., Godt, J. W., Bekins, B. A., & Rubinstein, J. L. (2015). High-rate injection is associated with the increase in U.S. mid-continent seismicity. *Science*, *348*(6241), 1336–1340. https://doi.org/10.1126/science.aab1345

Zhai, G., Shirzaei, M., & Manga, M. (2020). Elevated Seismic Hazard in Kansas Due to High-Volume Injections in Oklahoma. *Geophysical Research Letters*, *47*(5), 1–11. https://doi.org/10.1029/2019GL085705

Figure Captions

Figure 1. 49 Class I wells (red triangles) and 2381 Class II wells (blue triangles) dispose wastewater into the Arbuckle (size indicates cumulative injection into the well since 2000). The green polygons are areas where the Arbuckle wastewater injection is mostly balanced with hydrocarbon production. The yellow box shows south-central Kansas, where seismicity has surged markedly and a detailed geological and numerical model was constructed. The pressure profile for the wells that fall in the yellow polygon are used for history matching. Black dots correspond to M 3+ earthquakes from the USGS ComCat database.

Figure 2. Matching the measured Arbuckle pressures for wells (a) "KS-01-077-002", (b) "KS-01-173-001", and (c) "KS-01-173-002" (matched model 3; Table S14). Blue points are the historical pressure data, light blue curves show different simulation runs, and the red curve shows the best model determined by tuning the basement properties (permeability and porosity). More than 2000 runs are performed to obtain the best match.

Figure 3. Calculated crystalline basement porosity, permeability, specific storage and diffusivity for 10 different models.

Figure 4. (a-c) Cumulative pressure change (MPa) and (d-f) annual pressure change rate (MPa/year) across the south-central Kansas model area (Figure 1) since 2000, obtained from geological and numerical history matching. Vertical exaggeration is 10x.

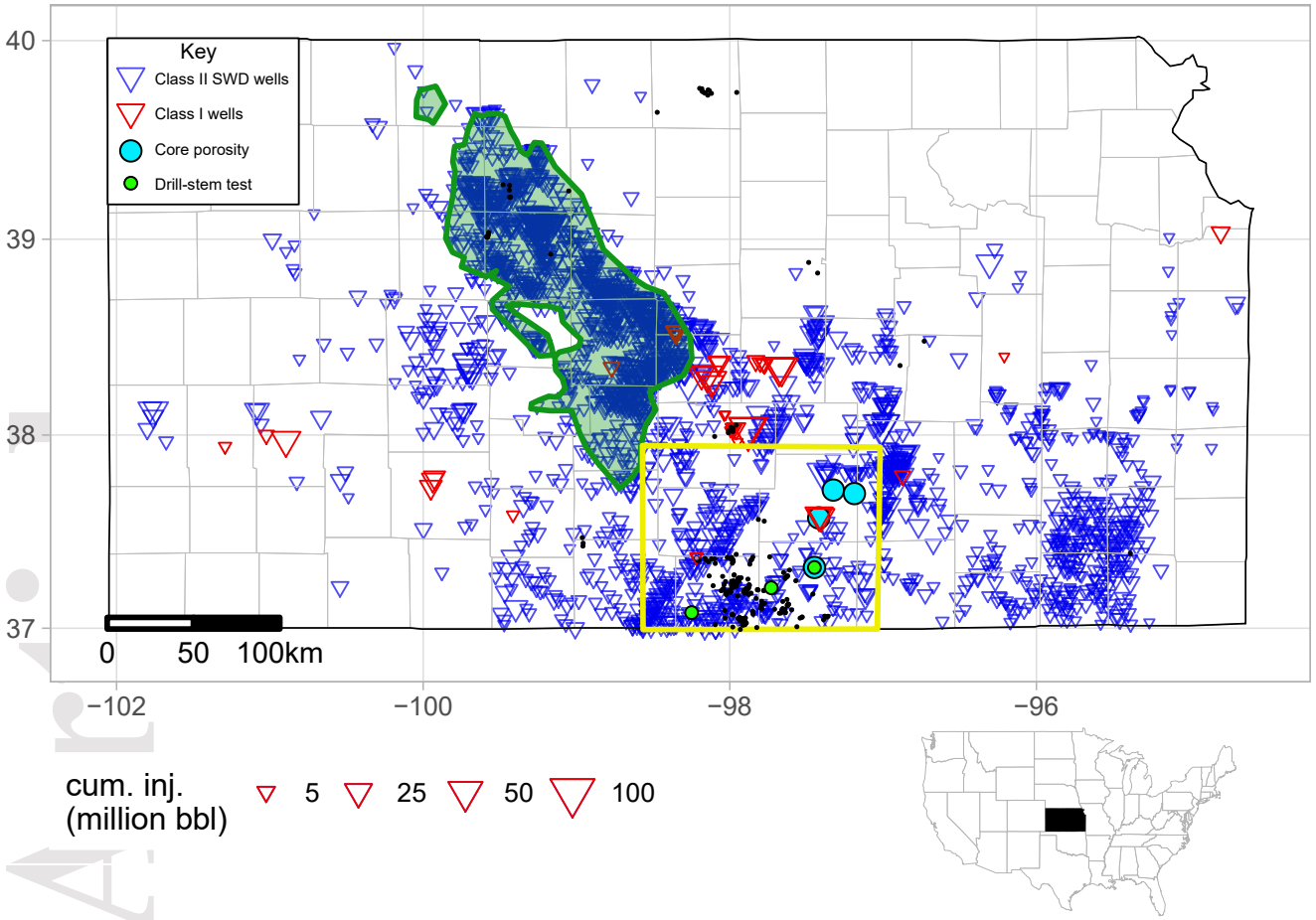

cum. inj. (million bbl) ▽ 5 ▽ 25 ▽ 50 ▽ 100